High-*np* Rydberg states of atomic carbon studied through vuv and uv double resonance

W. L. Glab and P. T. Glynn
Department of Physics, Texas Tech University, Lubbock, Texas 79409

F. Robicheaux
Department of Physics, Auburn University, Auburn, Alabama 36849
(Received 9 January 1998; revised manuscript received 20 May 1998)

We report on the use of an efficient stepwise-resonant two-photon excitation scheme to study high principal quantum number even-parity ($2pnp$) Rydberg states of atomic carbon. This scheme uses intense vacuum ultraviolet light to drive the resonance transition of the atoms, followed by excitation to Rydberg states with tunable ultraviolet light. Atomic carbon was produced under high vacuum conditions using laser ablation. Analysis of the spectrum of the unperturbed $J=3$ Rydberg series below and above the first ionization limit yielded a new value for the ionization potential of the atom, with an accuracy primarily limited by the accuracy with which the intermediate state energy is known. The spectra of the $J=0$, 1, and 2 Rydberg states all displayed the effects of coupling between different series converging to the two fine-structure states of the ion core. These spectra have been successfully reproduced using *ab initio* *R*-matrix calculations. [S1050-2947(98)09011-8]

PACS number(s): 32.80.Rm, 32.10.Hq, 31.15.Ar

INTRODUCTION

Although the spectroscopic study of atomic Rydberg states in the absence of external perturbations is in many ways a mature field, there are still a number of situations in which experimental data are lacking. These situations generally involve atoms with high ionization potentials (requiring the use of short-wavelength light for the excitation of their high-lying states) or atoms that are difficult to prepare in the vapor phase at high densities due to their high vaporization temperatures. Also, Rydberg states that are inaccessible from the ground state by single photon absorption due to parity restrictions are the least likely to have been studied in detail.

The spectrum of the carbon atom is of special importance for a number of applications, including studies of the interstellar medium [1] and the atmospheres of certain types of stars, the analysis of plasmas used in the production of carbon clusters such as fullerenes [2], and the study of energy losses due to impurities in fusion plasmas. In addition, recent years have seen the development of a number of laser-based schemes for the detection of atomic carbon in a variety of environments [3–8]. Despite this, the highly excited states of carbon have not yet been studied using modern laser spectroscopic techniques. A number of conventional absorption and emission spectroscopic studies have characterized the *ns*, *np*, *nd*, and *nf* singly excited states of the atom to principal quantum numbers of about 10, leading to a good understanding of the atom's term diagram and a rather accurate value for its ionization potential [9–11]. Such studies have typically been carried out in the somewhat violent environment of a carbon arc.

In this paper we will report on the first laser spectroscopic study of the high-*n* $2pnp$ even-parity Rydberg states of atomic carbon, and the comparison of the resulting experimental spectra to sophisticated *R*-matrix calculations. A beam of atomic carbon for the experiment was produced under high vacuum using laser vaporization of graphite. Step-

wise excitation of the Rydberg states was carried out using vacuum ultraviolet (vuv) excitation of the $2p3s$ upper states of the resonance transition, followed by further excitation using the ultraviolet (uv) light from a frequency-doubled tunable pulsed dye laser. Agreement between theory and experiment was generally excellent, although significant discrepancies between theoretical and experimental relative intensities were noted in several cases. These differences appear to be due to the presence of Cooper zeroes near threshold, and a consequent extreme sensitivity of the channel dipole matrix elements to the representation of the excited state wave functions. We conclude that the theoretical approach used in this work is capable of very accurately describing the highly excited states of this relatively simple system.

$2pnp$ Rydberg states of atomic carbon

Excitation of one of the $2p$ electrons from the ground state of carbon to an np orbital leads to a simple pp' system. For low principal quantum numbers, the spin-orbit interaction of this light atomic system is much weaker than the electrostatic direct and exchange interactions; consequently, the atom's low-lying states are well described in an *LS* coupling picture [12]. The resulting states are $^1S_0$, $^3S_1$, $^1P_1$, $^3P_{0,1,2}$, $^1D_2$, and $^3D_{1,2,3}$. In this coupling scheme, the total angular momentum of the ion core is not a good quantum number; consequently, the *LS* coupled series cannot, in general, be unambiguously associated with a particular ionic core spin-orbit fine-structure state. For high principal quantum numbers, the spin-orbit energy dominates the electrostatic energies, and a coupling scheme in which the total core angular momentum is a good quantum number, such as *jK* or *jj* coupling, is more appropriate. In this case each series of Rydberg states is associated with either the $^2P_{1/2}$ or the $^2P_{3/2}$ state of the ion core. The residual electrostatic interactions lead to couplings between Rydberg series with the same

value of J converging to distinct core states, leading to energy shifts due to interseries interaction.

In the experiment described in this paper, the Rydberg states are excited from each of the $2p3s$ $^3P_{0,1,2}$ states of the upper state of the atomic resonance transition. Depending on the particular intermediate state excited, various J values for the final Rydberg states are possible. In a jj-coupling picture, the following $2pnp$ Rydberg states are possible [using the notation $(j_c,j_e)_J$, where j_c is the total core angular momentum, j_e is the total angular momentum for the excited Rydberg electron, and J is the total angular momentum]: $(1/2,1/2)_0$, $(3/2,3/2)_0$, $(1/2,1/2)_1$, $(1/2,3/2)_1$, $(3/2,1/2)_1$, $(3/2,3/2)_1$, $(1/2,3/2)_2$, $(3/2,1/2)_2$, $(3/2,3/2)_2$, and $(3/2,3/2)_3$. Thus, for $J=0$ Rydberg states there is one series converging to the lower ($^2P_{1/2}$) state of the ion core and one series converging to the upper ($^2P_{3/2}$) state; for $J=1$, there are two series converging to each limit; for $J=2$, there is one series converging to the lower limit and two converging to the upper limit; and for $J=3$, there is a single series converging to the upper limit. This single $J=3$ series (which corresponds to $^3D_3$ in LS coupling) is particularly well suited for the precise determination of the energy interval between the $2p3s$ $^3P_2$ level and the $^2P_{3/2}$ ionization limit to which it converges, since it will be completely unperturbed. The series with other values of J will all display the effects of interseries interactions. These interactions can be approximately treated in a phenomenological fashion by setting up a diagonal energy matrix using the LS coupled representation energies for the system, and transforming this matrix to the jj coupled representation using the well known LS-jj transformation [12]. Channel quantum defects for the jj coupled series can then be extracted from the diagonal elements of the transformed matrix, and energy-scaled coupling matrix elements from the off-diagonal elements, thereby yielding the input data for a multichannel quantum defect theory (MQDT) model of the spectra. This procedure has been used previously for several systems, including the np Rydberg states of molecular hydrogen [13,14], although in that case the transformation is from Hund's case (b) to Hund's case (d) angular momentum coupling. Rather than this phenomenological approach, for this study we chose to compare the experimental data with sophisticated R-matrix calculations, in which the spin-orbit coupling was taken into account using the LS-jj transformation. The theoretical approach, which has been described in detail elsewhere [15–17], will be sketched below. The expectation was that, given the simplicity of the pp' system, good agreement could be obtained between experiment and such a fully *ab initio* theory. This expectation was largely borne out in this study.

EXPERIMENT

The experiment used stepwise resonant, two-photon excitation followed by pulsed electric field ionization to excite and ionize high principal quantum number Rydberg states of the carbon atom. Since the laser vaporization scheme described below produced rather low densities of atomic carbon at the location of the interrogating laser beams, an efficient approach of excitation was required. The scheme chosen for this work involved pumping the atoms from the ground state to the $2p3s$ ^3P $J=0$, 1, or 2 state using tunable
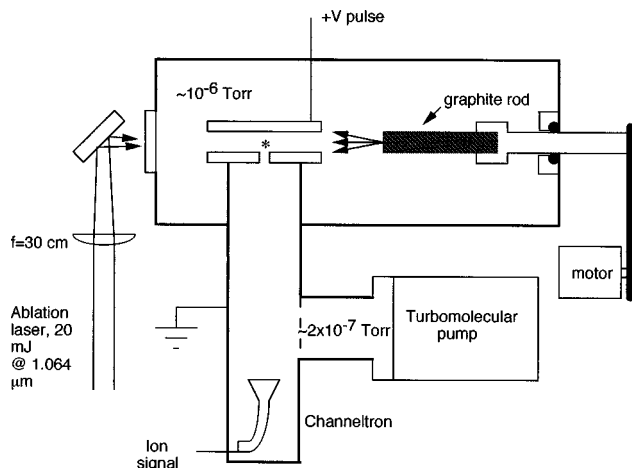

FIG. 1. A schematic diagram of the laser-vaporization–time-of-flight mass spectrometer apparatus. The vuv and uv probe laser beams enter the chamber on an axis perpendicular to the plane of the figure, as indicated by the asterisk.

vuv light produced by two-photon resonant difference-frequency generation in xenon gas. Once the atoms were excited to a particular angular momentum state of the $2p3s$ state, they were further excited to the region of the ionization limit by a second tunable, frequency-doubled dye laser. The experiment detected carbon ions formed either from pulsed electric ionization or autoionization of the resulting high Rydberg states.

Figure 1 shows a schematic diagram of the carbon vapor source and laser ionization chamber. The vacuum layout consisted of two regions: the sample region which contained the laser vaporization source and the ion extraction plates for the time-of-flight mass spectrometer, and the vacuum region of the time-of-flight drift tube and the channeltron ion detector. The graphite rod, which served as the carbon source, was mounted on a vacuum rotary feedthrough in such a way that its flat end faced the window through which the ablation laser pulses entered the chamber. No special processing of the rod face was done before the experiment was undertaken. An electric motor drove the rotation of the rod at 5 rpm. The face of the rod was a distance of 3 cm from the edge of the time-of-flight ion extraction plates, which were 5 cm in diameter and spaced by 2 cm.

The graphite was vaporized by 20-mJ pulses of 1.064-μm light with 5-ns duration and 10-Hz repetition rate from a compact Nd^{3+}:YAG laser (Continuum Minilite). This ablation light was focused onto the rod using a 30-cm focal length lens. The best experimental results, in terms of an optimum balance between atomic carbon density and pulse-to-pulse density stability, was achieved when the spot of light was slightly defocused on the rod. The largest carbon density at the location of the ion extraction region occurred when the delay between the ablation laser and the probe lasers was ~120 μs, which is consistent with a translational temperature of roughly 4000 K for the ablation plume as has been observed before under similar conditions [18].

The time-of-flight plates were electrically grounded when the probe laser pulses arrived, so that the Rydberg states were excited under field-free conditions; 50 ns after the probe laser pulses, a 150-V/cm field pulse was applied to
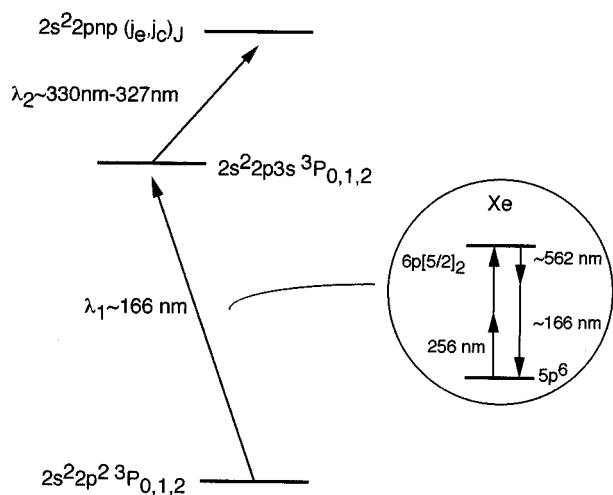
FIG. 2. Excitation scheme for resonant stepwise two-photon excitation of $2pnp$ Rydberg states of carbon. The inset shows the xenon levels and laser wavelengths involved in the production of 166-nm vuv light through difference frequency generation.
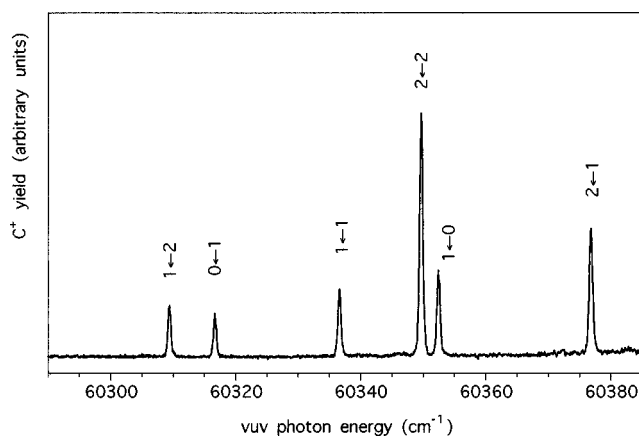

FIG. 3. The spectrum of $2p3s\ {}^3P_{J'}\leftarrow 2p^2\ {}^3P_{J''}$ transitions observed by scanning the vuv photon energy. The peaks are labeled with the lower state J'' and upper state J' as $J'\leftarrow J''$.

field ionize high-n Rydberg state atoms and drive the resulting ions into the flight tube of the time-of-flight mass spectrometer. Carbon ions were identified by their time-of-flight after separation from the large background of ions from the ablation process and photodegradation and ionization of organic impurities.

The xenon cell used for vuv generation was mounted on the vacuum chamber in such a way that the probe laser beams, the expanding carbon atom plume, and the axis of the time of flight were all mutually orthogonal. The design of the cell was very simple, consisting of a $2\frac{3}{4}$-inch Conflat flange tee with a fused silica entrance window and a plane-parallel MgF_2 output window mounted with a vacuum tight seal on a double-sided flange between the cell and the vacuum system. The cell was first evacuated through the third arm of the tee with a mechanical pump, then filled with 15 Torr of xenon gas as measured by a capacitance manometer.

Figure 2 schematically shows the excitation process on a partial energy level diagram of carbon, as well as the difference-frequency generation scheme used to produce the vuv light to drive the first excitation step. Two homebuilt dye lasers pumped by a single Q-switched Nd^{3+}:YAG laser (Continuum NY-61, producing $\sim$5-ns-long pulses of light at 532 and 355 nm at a 10-Hz repetition rate) were used to produce light at the fundamental wavelengths required to drive the two-photon resonant difference-frequency generation process in xenon [19,20] for the production of the 166-nm vuv light. The first of these lasers, pumped by the third harmonic light at 355 nm from the Nd^{3+}:YAG laser, operated at 512 nm, producing 7-mJ pulses of light with $\sim$4-ns duration and a bandwidth of $\sim$0.03 cm^{-1}. This light was frequency doubled using a BBO crystal to yield pulses of light at 256 nm with $\sim$0.5-mJ energy. This light was tuned into resonance with the $5p^6\rightarrow\rightarrow 5p^66p[5/2]_2$ two-photon transition in xenon by observing $2+1$ ionization in the xenon cell. Light of the second wavelength required for the vuv generation came from a second dye laser pumped by the second harmonic of the same Nd^{3+}:YAG laser. This dye laser, which was of a simpler design than the first and con-

sequently produced light with a somewhat greater bandwidth ($\sim$0.2 cm^{-1}), was tunable near 562 nm and produced 2 mJ pulses. The light from this laser was sent through a telescope, which made it possible to adjust its divergence to improve the matching of the locations of the beam waists after the the beams were focused into the xenon cell. After the beams were combined with a dichroic mirror, the light was focused into the xenon cell with a 15-cm focal length fused silica lens. The combined fundamental lights and generated vuv were allowed to expand out from the focus, pass through the MgF_2 window, and pass to the interaction region of the time-of-flight mass spectrometer. The bandwidth of the vuv light was estimated to be less than 0.3 cm^{-1}, and the beams had a diameter of about 2 mm at the interaction region. Although we did not measure the pulse energy of the generated vuv light, previous work done under similar conditions [20] would lead us to expect that about 10^{11} photons/pulse were produced. If so, the vuv photon flux would have been large enough to nearly saturate the resonance line transitions.

The light required to excite the high np Rydberg states (or photoionize the atoms for photon energies above that required for direct photoionization) was produced by frequency doubling the output of a third, homebuilt tunable dye laser, operating in the wavelength region near 660 nm and producing 8-mJ pulses of light with a bandwidth of about 0.03 cm^{-1}. An autotracking device (INRAD AT-II) was used to maintain proper phase matching as the wavelength of the laser output was scanned over the region of interest. The frequency-doubled output pulse energy delivered to the interaction region was about 0.5 mJ/pulse in a 3-mm-diameter beam, and was delayed from the vuv pulse by about 10 ns.

Figure 3 shows a scan of the vacuum ultraviolet photon energy over the various allowed resonance line transitions, with the ionizing laser wavelength set to give a photon energy sufficient to ionize the excited atoms leaving the core in either spin-orbit state. The transitions are marked as $J'\leftarrow J''$, where J'' is the total angular momentum of the initial ground-state level and J' is the total angular momentum of the $2p3s$ excited-state level. The spectrum shows that the first step transitions are well resolved and can be efficiently excited with our vuv source. The linewidths of $\sim$0.5 cm^{-1} are due to the vuv laser bandwidth and Doppler broadening

in the expanding carbon sample.

Spectra were acquired using a personal computer, which controlled the laser wavelength scanning and recorded the ion yield for each laser shot. A dozen laser shots were averaged for each wavelength of the spectra to reduce noise. The laser intensities were not monitored, since the primary source of fluctuations and drift in the signal size was the density of ablated carbon. A calibration spectrum of fluorescence from molecular iodine was acquired simultaneously with the ionization spectrum. The iodine spectra were subsequently used to calibrate the photon energies for the ionization spectra to an accuracy of about 0.05 cm^{-1} in the full doubled dye laser energy.

Theoretical approach

Generic features

The calculations are performed using the variational R-matrix method [21] as implemented in Refs. [15] and [16]. The orbitals for the core electrons are generated using Froese-Fischer's configuration average Hartree-Fock programs [22] and are input into the R-matrix codes. All other orbitals are generated using the direct part of the Hartree potential. Twenty orbitals per 1 were used; nineteen of the orbitals are set to zero at the surface of the R-matrix volume and one of the orbitals had zero derivative. The surface of the R-matrix volume was chosen to be 23 bohr radii. The solutions of the R-matrix equations were matched to Coulomb waves outside of the R-matrix volume so the channel interactions were only included out to 23 a.u.; this should be an excellent approximation. This calculation gave us the LS-coupled dipole matrix elements and K matrices that describe the channel interaction.

The spin-orbit interaction was included only for the core electrons. This was incorporated using an LS-to-jj frame transformation on the calculated K matrices and dipole matrix elements [15–17]. To this point the calculations are completely *ab initio*. In order to obtain sub-cm^{-1} agreement with experiment, we used the experimental threshold positions as input into the multichannel quantum defect equations.

An important feature of the calculation is the use of the preconvolution technique [23] for computing photoabsorption spectra. Most of the experimental spectra are in the bound-state region and thus the usual implementation of MQDT is not possible. With the usual MQDT procedure, a search for the energy positions of the bound states would be necessary. This would be followed by taking energy derivatives of dipole matrix elements and K matrices at the energy of the state. With the preconvolution technique, the cross section is calculated by stepping in energy and solving a linear matrix equation similar to the usual calculations performed in the autoionization regime. All that is needed as input is the experimental energy resolution; the result is a direct computation of the convolved photoabsorption cross section without the need for first calculating an unconvolved cross section.

Calculation

The initial state of C was not the ground state but the much more diffuse $2s^2 2p3s$ ^3P state. This caused some dif-

ficulties in the calculation as compared to our previous calculation for C [21]. The main difficulty was that the R-matrix volume needed to be much larger in order to contain the initial state. There was also difficulty because this state could mix with other states with nearly the same energy (for example, $2s2p^3$ and $2s^2 2p3d$). Another difficulty is that in both the $2pnp$ ^3S and ^3P channels there are Cooper zeros just outside of the energy range of interest; the Cooper zero is just below our energy range for the ^3S channel and just above our energy range for the ^3P channel. This is reflected in the large difference between the length and velocity dipole matrix elements that we calculated; the error was up to 50% in some channels.

The channel couplings and quantum defects are much more accurate than the dipole matrix elements. For all LS-coupled symmetries except the ^1D and ^3D, there is only one channel. For the ^1D and ^3D channels we performed two channel calculations including the $2pnp$ and $2pnf$ series. However, the channel couplings were so weak and the oscillator strength to the $2pnf$ states was so small that the results were not visibly changed if the $2pnf$ series were not included in the calculation.

Although there is only one physical series per LS symmetry we included a number of other channels in the R-matrix calculation to incorporate relaxation, configuration interaction, and polarizability. The main series was $2s^2 2pnp$. Relaxation effects were incorporated through $2s^2 3pnp$ and $4pnp$ basis functions. Correlation was incorporated through $2p3d^2 np$, $2p^3 np$, and $2p^4$ basis functions as well as $2s2p3snp$ and $2s2p3dnp$ basis functions. Polarizability and correlation were incorporated through $2s2p^2 ns$ and nd basis functions, $2s3d^2 ns$ and nd basis functions, as well as $2s^2 3dnd$ basis functions. Many other types of basis functions were also included.

We now present some intermediate results of the calculations. The $1/r_{12}$ matrix contains information on the electrostatic interactions between the excited electron and the remaining $1s$, $2s$, and $2p$ electrons at short range, where the LS-coupled channels are the appropriate description for the wave function. These electrostatic terms give rise to the short-range eigenchannel quantum defects. The terms that vary from one LS-coupled channel to another are the direct quadrupole, exchange monopole, and exchange quadrupole terms. The radial parts of the matrix elements for these interactions were calculated to be 9.38, 2.63, and 2.75, respectively, in arbitrary units. Table I gives the angular parts of each of these matrix elements for each LS-coupled channel, as well as the total $1/r_{12}$ matrix elements (obtained by summing the products of the radial and angular parts of the three matrix elements), and the calculated quantum defect for each LS-coupled channel. Generally, the quantum defect decreases with increasing V (increasing total energy) as would be expected from the modified Rydberg formula including the quantum defect.

Table II presents the K matrices used in the calculation in the LS-coupled basis, the configurations contributing to each channel, and the dipole matrix elements for each channel in both the length and velocity formalisms. For the ^1D and ^3D channels both εp and εf configurations are included, although it is apparent from the magnitudes of the diagonal elements of the K matrices that the contributions of the εf

4018 W. L. GLAB, P. T. GLYNN, AND F. ROBICHEAUX PRA 58

TABLE I. Contributions of the direct quadrupole (DQ), exchange monopole (EM), and exchange quadrupole (EQ) terms to the angular part of the $1/r_{12}$ matrix elements in arbitrary units, as well as the total matrix element V and resulting quantum defect μ for the LS coupled channels.

LS channel	DQ	EM	EQ	V	μ
^1S	0.4	1.0	0.4	7.48	0.39
^1D	0.04	1.0	0.04	3.12	0.49
^3S	0.4	−1.0	−0.4	0.02	0.63
^3D	0.04	−1.0	−0.04	−3.35	0.66
^1P	−0.2	−1.0	0.2	−3.96	0.70
^3P	−0.2	1.0	−0.2	0.20	0.72

TABLE III. The jj-coupled K matrix in arbitrary units. The rows and columns are in the following order: $j_c = 1/2$, $j_e = 1/2$; $j_c = 1/2$, $j_e = 3/2$; $j_c = 3/2$, $j_e = 1/2$; and $j_c = 3/2$, $j_e = 3/2$.

$$\begin{pmatrix} -1.696 & 0.007 & -0.007 & 0.213 \\ 0.007 & -7.161 & -5.102 & -0.312 \\ -0.007 & -5.102 & -7.161 & 0.312 \\ 0.213 & -0.312 & 0.312 & -1.785 \end{pmatrix}$$

configurations is very small compared to the εp configurations. All of the oscillator strength for the transitions from the $2p3s$ initial states to the final LS-coupled channels is taken to reside in the transitions to the triplet states obeying the selection rule $\Delta L = 0, \pm 1$, as anticipated for a light atom whose low-lying states are well described by LS coupling. The reason for the significant discrepancies between the dipole matrix elements in the velocity and length formalisms was discussed above.

Table III gives the jj-coupled K matrix for the $J = 1$ final states. It is evident that the largest coupling between the different jj-coupled channels is between the $j_c = 1/2$, $j_e = 3/2$ $[(1/2,3/2)_1]$ and the $j_c = 3/2$, $j_e = 1/2$ $[(3/2,1/2)_1]$ channels. The two series converging to the lower ionization limit have a very small coupling; as a result, these two Rydberg series are unusually pure jj states away from perturbations, as will be noted in more detail below. All of the other interseries couplings are down from the $j_c = 1/2$, $j_e = 3/2 \leftrightarrow j_c = 3/2$, $j_e = 1/2$ coupling by more than an order of magnitude. A further detailed comparison between the calculated results for the $J = 1$ final states and the experimental results will be given in the next section.

EXPERIMENTAL RESULTS AND COMPARISON TO THEORY

Figure 4 shows a portion of the spectrum of Rydberg states excited from the $2p3s$ $^3P_2$ level as a function of the

frequency-doubled dye laser wavelength. One prominent series of Rydberg states, $np(3/2,3/2)_3$ in jj coupling or $^3D_3$ in LS coupling, appears in the ion spectrum, converging to the $^2P_{3/2}$ core state ionization limit. The nonmonotonic variation in the peak heights is due to changes in the ablated carbon density during the acquisition of this spectrum. The $np(3/2,3/2)_3$ series is the only possible $J = 3$ Rydberg series that can arise in the pp' system represented by carbon, a fact that has several consequences. First, this means that the series will have no perturbers satisfying the $\Delta J = 0$ selection rule (ignoring the possible effects of doubly excited states of different configurations) and should be accurately describable with a Rydberg formula with a constant (or nearly constant) quantum defect. For this reason, this series is well suited for a determination of the ionization energy of the carbon atom. Also, these states will not autoionize since there is no $J = 3$ continuum with which to couple; therefore, we must be observing this series through pulsed electric field ionization, and the linewidths for this series (~ 0.15 cm^{-1}) represent the experimental resolution. Members of this series with $n \leq 10$ were in fact used for the best previous determination of the ionization energy of carbon [11]. We observe these states clearly to much higher principal quantum numbers than in the conventional work of Ref. [11], so an improved value for the energy interval between the $2p3s$ $^3P_2$ state and the $^2P_{3/2}$ ionization limit can be extracted from our results. Taken together with the best known value for the energy interval between the ground state and the $2p3s$ intermediate state and the spin-orbit splitting of the ion states, a new value for the ionization energy of carbon can be derived.

For the ionization energy determination we used the mea-

TABLE II. The LS-coupled K matrices and dipole matrix elements used in the calculation (arbitrary units).

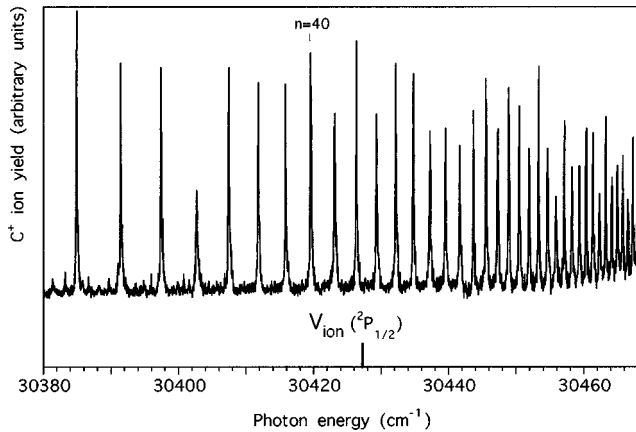| LS channel	K-matrix elements	Configuration	d (length)	d (velocity)
^1S	2.78	$2p\varepsilon p$	0	0
^1P	−1.37	$2p\varepsilon p$	0	0
^1D	$\begin{pmatrix} 21.4 & -0.33 \\ -0.33 & -0.0077 \end{pmatrix}$	$2p\varepsilon p$ $2p\varepsilon f$	0 0	0 0
^1F	0.046	$2p\varepsilon f$	0	0
^3S	−2.41	$2p\varepsilon p$	−0.93	−1.29
^3P	−1.24	$2p\varepsilon p$	−15.3	−16.4
^3D	$\begin{pmatrix} -1.76 & 0.018 \\ 0.018 & -0.014 \end{pmatrix}$	$2p\varepsilon p$ $2p\varepsilon f$	−3.82 0.17	−4.08 0.21
^3F	0.045	$2p\varepsilon f$	0	0
^3G	−0.0023	$2p\varepsilon f$	0	0

FIG. 4. Spectrum of Rydberg states excited from the $2p3s$ $^3P_2$ level. The carbon ion yield is plotted versus the doubled dye laser (uv) photon energy. The ionization energy of carbon is marked on the horizontal axis. The prominent series converging to the $^2P_{3/2}$ limit is $(3/2,3/2)_3$ in jj coupling or $^3D_3$ in LS coupling, observed through pulsed electric field ionization.

sured transition energies from the $2p3s$ $J=2$ state to the $np(3/2,3/2)_3$ states with n between 35 and 70; for improved accuracy, we averaged values for the energies as determined from two separate spectra. The state energies derived from the two different runs agreed to within 0.05 cm^{-1} in most cases. The energies were then fit to a simple Rydberg formula

$$E_n = V_{ion}(^2P_{3/2}) - \frac{\mathcal{R}_C}{(n-\delta)^2},$$

where E_n is the transition energy to the Rydberg state with principal quantum number n, $V_{ion}(^2P_{3/2})$ is the energy difference between the $2p3s$ $J=2$ state and the ionization limit for the $^2P_{3/2}$ ionic state, $\mathcal{R}_C$ is the Rydberg for atomic carbon (109 732 cm^{-1}), and δ is the quantum defect for the $np(3/2,3/2)_3$ series. We used a two-parameter fit in which $V_{ion}(^2P_{3/2})$ and δ were allowed to vary, with the results $\delta = 0.673 \pm 0.01$ and $V_{ion}(^2P_{3/2}) = 30\,490.54 \pm 0.03$ cm^{-1}. The residuals from this fit were at most 0.1 cm^{-1}, and in most cases less than 0.05 cm^{-1}. The first result is consistent with the quantum defect determined in Ref. [11] for high n, 0.676. The second result, taken together with the result for the $2p3s$ $J=2$ state energy from Ref. [11], 60393.14$\pm$0.05 cm^{-1}, gives an improved value for the energy difference between the neutral ground state and the $^2P_{3/2}$ ionization limit of 90 883.68$\pm$0.08 cm^{-1}. This is in marginal agreement with the slightly less accurate value of 90 883.84$\pm$0.1 cm^{-1} of Ref. [11]. If we combine our value with the energy splitting between the ionic $^2P_{1/2}$ and $^2P_{3/2}$ states [24] from far-IR laser magnetic resonance, 63.35 cm^{-1}, we obtain a value for the ionization energy of carbon of 90 820.33$\pm$0.08 cm^{-1}, in agreement with the value of 90 820.42$\pm$0.1 cm^{-1} of Ref. [11]. Although our result has only slightly higher accuracy than the previous value, we should point out that most of the imprecision comes from our knowledge of the $2p3s$ initial-state energy. A more accurate determination of the $2p3s$
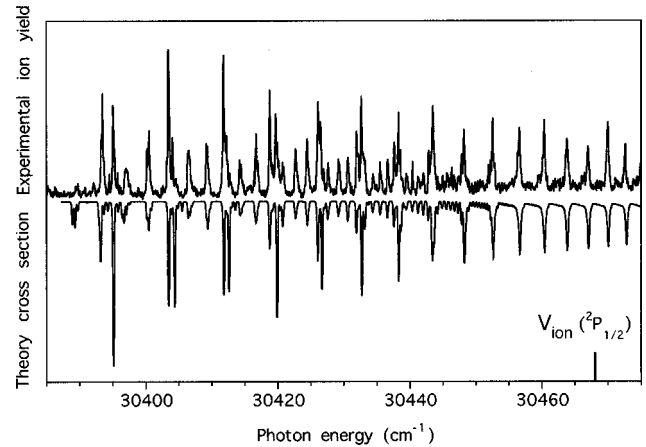

FIG. 5. Spectrum of $J=1$ Rydberg states excited from the $2p3s$ $^3P_0$ level. The top trace is the experimental spectrum, while the lower, inverted trace is the theoretical prediction. The details of these spectra are discussed in the text.

energy would allow a more accurate ionization energy to be determined, with an accuracy of up to three times better than the best previous value.

As another check of the accuracy of our fitted results, we also tried fitting the observed energies to a formula that included a parameter that allowed the quantum defect to vary linearly with energy, as it might over the small energy range under consideration if there were a strong perturber (i.e., a doubly excited state) affecting the spectrum. This fit gave an ionization energy result that differed from the constant quantum defect result by only 0.01 cm^{-1}, and a value for the quantum defect variation slope (1/cm^{-1}) which was consistent with zero. We conclude that the spectrum of the $^3D_3$ states is very well described by the simple Rydberg formula given above.

The Rydberg spectra from the other two $2p3s$ levels show strong series converging to each of the two lowest ionization potentials of the atom. Figure 5 shows the spectrum of np $J=1$ final states excited from the $2p3s$ $^3P_0$ level. The top spectrum is the experimental spectrum, while the lower, inverted spectrum shows the results of the theoretical calculation described above. The theoretical calculation reproduces the energy positions of the Rydberg states (through the quantum defects) and the general appearance of the spectrum very well. As discussed above, we would expect to see two series converging to each ionization limit for the $J=1$ Rydberg states. While the spectra clearly show two series converging to the $^2P_{3/2}$ ion core state limit, only one strong series is seen converging to the lower, $^2P_{1/2}$ limit. This is because the second series ($j_c = 1/2$, $j_e = 3/2$) converging to the lower limit has about a factor of ten smaller oscillator strength than the $j_c = 1/2$, $j_e = 1/2$ series. The only locations where the weaker series plays a significant role in the spectrum is in regions of strong interseries interactions, where the $^2P_{1/2}$ series are perturbed strongly by the nearly degenerate states of the $^2P_{3/2}$ series. In these regions, the weak series gives rise to an extra peak due to intensity borrowing from the perturbing states. An interesting feature of the two series attached to the $j_c = 1/2$ limit is their purity; usually, when there are two series attached to the same threshold there is a degree of mixing of the series that is
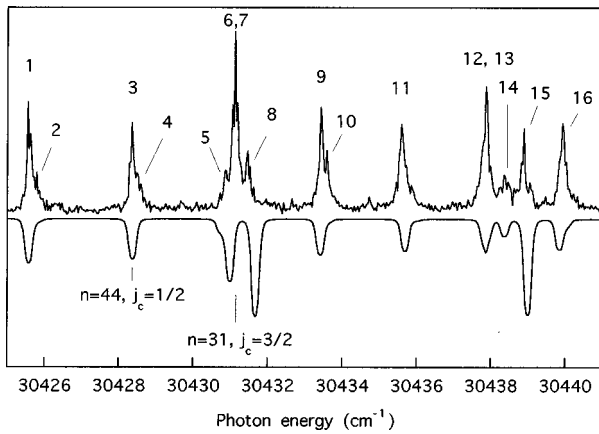
FIG. 6. An expanded region of Fig. 5. The peaks are labeled with numbers that refer to Table IV.

roughly constant with n. In the case of the $2pnp$ $j_c=1/2$ series in carbon, the calculations indicate that the series are roughly 97–99% pure away from perturbers.

Figure 6 shows an expanded region of the Rydberg spectrum of $J=1$ final states compared to the theoretical calculation. Table IV gives additional information on the states responsible for the peaks that are numbered in the figures, including their theoretical oscillator strengths and percentage channel compositions in the jj coupling scheme basis. The LS compositions are also given for the states that are in regions of strong interseries interaction. The high purity of the Rydberg series converging to the $j_c=1/2$ limit away from perturbers is evident in the table, as is the strongly mixed

nature (in the jj basis) of those states near interseries near degeneracies.

While the theoretical calculation gives remarkable agreement with the experimental results for the state positions, the agreement for the relative intensities of the series is not as good. In particular, the theoretical result for the series converging to $^2P_{1/2}$ is about one-half the experimental result, relative to the strongest $^2P_{3/2}$ series. This is apparent both in the discrete spectrum and in the autoionization region, where the experimentally observed continuum is considerably stronger than predicted by theory. Also, the intensity ratio between the two $^2P_{3/2}$ series is off by a factor of about two. This appears to be due to the extreme sensitivity of the dipole matrix elements to the excited-state wave function due to the presence of Cooper zeroes in the ^3S and ^3P channels, as discussed above. It is also possible that there is some degree of saturation of the second-step transitions to the higher-intensity Rydberg states, although that should lead to significant broadening of the resonances, which we do not observe. It is fair to say that the agreement between experiment and theory is very good for this simple pp' system.

Figure 7 shows the spectrum of $J=0$, 1, and 2 states excited from the $2p3s$ $^3P_1$ level. Comparison to the theoretical predictions shows that the prominent peaks in this spectrum belong to $J=2$ states, although some of the smaller features are due to excitation of $J=1$ states. For $J=2$ Rydberg states we expect one series converging to the $^2P_{1/2}$ limit and two converging to the $^2P_{3/2}$ limit; in fact, the spectrum looks much the way we would expect it to if this were the case. The peaks converging to the lower limit, however, are

TABLE IV. Energies, calculated oscillator strengths f, and channel compositions of the $J=1$ states labeled in Fig. 6. LS compositions are given for those states for which LS coupling is a better description than jj coupling. For the jj-coupled designations, (1,1) denotes $j_c=1/2$, $j_e=1/2$, (1,3) denotes $j_c=1/2$, $j_e=3/2$, and so on.

| Label	E (cm^{-1})	f (arb. units)	jj composition	LS composition
1	30 425.65	10.0	(1,1) 99.9%	
2	30 425.94	0.5	(1,3) 98% (3,1) 2%	
3	30 428.46	9.1	(1,1) 98%	
4	30 428.66	0.04	(1,3) 98% (3,1) 1.5%	
5	30 430.83	2.8	(3,3) 68% (1,3) 15%	
			(3,1) 10% (1,1) 8%	^1P 96%
6	30 431.08	14.1	(1,1) 88% (1,3) 8%	^3D 95% ^1P 4%
7	30 431.22	0.1	(1,3) 57% (3,3) 28%	
			(3,1) 10% (1,1) 5%	^3S 90% ^3P 10%
8	30 431.75	22	(3,1) 74% (1,3) 24%	
			(3,3) 2%	^3P 91% ^3S 8%
9	30 433.51	8.2	(1,1) 99.9%	
10	30 433.73	0.5	(1,3) 98% (3,1) 2%	
11	30 435.77	7.3	(1,1) 99.7%	
12	30 437.90	4.5	(1,1) 94% (1,3) 3%	
13	30 438.01	3.4	(1,3) 83% (3,1) 6%	
			(3,3) 5% (1,1) 4%	
14	30 438.45	3.9	(3,3) 86% (1,3) 11% (3,1) 2%	
15	30 439.08	22	(3,1) 85% (1,3) 10%	
			(3,3) 5%	^3P 76% ^3S 23%
16	30 439.92	6.8	(1,1) 99.8%	
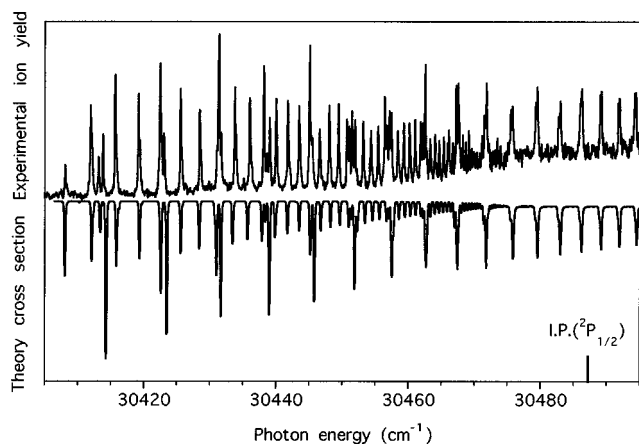
FIG. 7. Spectrum of $J=0$, 1, and 2 Rydberg states excited from the $2p3s$ $^3P_1$ level, presented as in Fig. 5.

broader than the experimental resolution and sometimes show substructure. This is reproduced in the theoretical calculations, which show that these features of the spectra are due to overlapping $J=1$ Rydberg states that have almost the same quantum defect as the $J=2$ series. The variation of peak heights for the series converging to the $^2P_{1/2}$ state of the ion, in regions of perturbation by the series converging to the $^2P_{3/2}$ ion state, are also reproduced by the theory, an indication that the interseries coupling has been accurately determined in the theory in both magnitude and sign. As in the case of the spectrum in Fig. 5, and for the same possible reasons, the intensities of the peaks due to the series converging to the $^2P_{1/2}$ limit are underestimated by the theory.

CONCLUSIONS

We have demonstrated an extremely efficient two-step vuv+uv excitation scheme for highly excited $2pnp$ states of atomic carbon, a sample of which was produced in vacuum by the laser vaporization of graphite. The vacuum ultraviolet light near 166 nm required to pump the resonance line transitions of atomic carbon was produced using two-photon resonant difference-frequency generation. From an analysis of the spectrum of unperturbed $2pnp$ $J=3$ Rydberg states we redetermined the ionization energy of carbon, finding a value in agreement with the best previous value and somewhat more accurate. If more precise values for the $2p^2$-$2p3s$ energy intervals were to become available, a still more accurate value for the ionization energy could be found from our result. $J=0$, 1, and 2 Rydberg series excited from the $2p3s$ $^3P_{0,1}$ levels showed interactions between series converging to the two spin-orbit split energy levels of the ground state of the carbon ion. These experimental spectra were compared with the results of sophisticated *ab initio* R-matrix calculations, and very good agreement between experiment and theory were seen. The experimental approach can be readily extended to larger carbon species or atomic and molecular species involving other refractory elements. Isotopic selectivity could easily be achieved if the laser resolution were improved, and one could imagine applications of this approach to isotopic analysis of carbon in solids and on surfaces.

[1] H. E. Payne, K. R. Anantharamaiah, and W. C. Erickson, Astrophys. J. **430**, 690 (1994).

[2] E. A. Rohlfing, J. Chem. Phys. **89**, 6103 (1988).

[3] R. C. Sausa, A. J. Alfano, and A. W. Miziolek, Appl. Opt. **26**, 3588 (1987).

[4] K. H. Becker, K. J. Brockman, and P. Wiesen, J. Chem. Soc., Faraday Trans. 2 **84**, 455 (1988).

[5] P. J. H. Tjossen and K. C. Smyth, Chem. Phys. Lett. **144**, 51 (1988).

[6] H. Bergstrom, H. Halstadius, H. Lundberg, and A. Persson, Chem. Phys. Lett. **155**, 27 (1989).

[7] M. Alden, P.-E. Bengtsson, and U. Westblom, Opt. Commun. **71**, 263 (1989).

[8] U. Westblom, P.-E. Bengtsson, and M. Alden, Appl. Phys. B: Photophys. Laser Chem. **52**, 371 (1991).

[9] G. Herzberg, Proc. R. Soc. London, Ser. A **248**, 309 (1958).

[10] V. Kaufman and J. Ward, J. Opt. Soc. Am. **56**, 1591 (1966).

[11] L. Johansson, Ark. Fys. (Stockholm) **31**, 201 (1966).

[12] I. I. Sobelman, *Atomic Spectra and Radiative Transitions* (Springer-Verlag, Berlin, 1979).

[13] G. Herzberg and Ch. Jungen, J. Mol. Spectrosc. **41**, 425 (1971).

[14] W. L. Glab, K. Qin, and M. Bistransin, J. Chem. Phys. **102**, 2338 (1995).

[15] F. Robicheaux and C. H. Greene, Phys. Rev. A **46**, 3821 (1992).

[16] F. Robicheaux and C. H. Greene, Phys. Rev. A **47**, 4908 (1993).

[17] M. Aymar, C. H. Greene, and E. Luc-Koenig, Rev. Mod. Phys. **68**, 1015 (1996).

[18] R. W. Dreyfus, R. Kelly, and R. E. Walkup, Nucl. Instrum. Methods Phys. Res. B **23**, 557 (1987).

[19] G. Hilber, A. Lago, and R. Wallenstein, J. Opt. Soc. Am. B **4**, 1753 (1987).

[20] J. Hager and S. C. Wallace, Chem. Phys. Lett. **90**, 472 (1982).

[21] C. H. Greene, Phys. Rev. A **32**, 1880 (1985).

[22] C. Froese-Fischer, Comput. Phys. Commun. **4**, 107 (1972).

[23] F. Robicheaux, Phys. Rev. A **48**, 4162 (1993).

[24] A. L. Cooksy, G. A. Blake, and R. J. Saykally, Astrophys. J. **305**, L89 (1986).